3-2012

Synoptic-Scale Environments Conducive to Orographic Impacts on Cold-Season Surface Wind Regimes at Montreal, Quebec

Alissa Razy
Israel Meteorological Service

Shawn M. Milrad
McGill University, milrads@erau.edu

Eyad H, Atallah
McGill University

John R. Gyakum
McGill University

Scholarly Commons Citation

Razy, A., Milrad, S. M., Atallah, E. H., & Gyakum, J. R. (2012). Synoptic-Scale Environments Conducive to Orographic Impacts on Cold-Season Surface Wind Regimes at Montreal, Quebec. *Journal of Applied Meteorology and Climatology, 51*(3). https://doi.org/10.1175/JAMC-D-11-0142.1

Synoptic-Scale Environments Conducive to Orographic Impacts on Cold-Season Surface Wind Regimes at Montreal, Quebec

ALISSA RAZY,* SHAWN M. MILRAD, EYAD H. ATALLAH, AND JOHN R. GYAKUM

Department of Atmospheric and Oceanic Sciences, McGill University, Montreal, Quebec, Canada

(Manuscript received 13 July 2011, in final form 4 November 2011)

ABSTRACT

Orographic wind channeling, defined as dynamically and thermally induced processes that force wind to blow along the axis of a valley, is a common occurrence along the St. Lawrence River Valley (SLRV) in Quebec, Canada, and produces substantial observed weather impacts at stations along the valley, including Montreal (CYUL). Cold-season observed north-northeast ($n = 55$) and south-southeast ($n = 16$) surface wind events at CYUL are identified from 1979 to 2002. The authors partition the north-northeast wind events into four groups using manual synoptic typing. Types A and D (''inland cyclone'' and ''northwestern cyclone'') are associated with strong lower-tropospheric geostrophic warm-air advection and near-surface pressure-driven channeling of cold air from the north-northeast, along the axis of the SLRV. Type C (''anticyclone'') shows no evidence of a surface cyclone and thus is the least associated with inclement weather at CYUL, whereas type B (''coastal cyclone'') is associated with predominantly forced wind channeling along the SLRV. Type D of the north-northeast wind events and all south-southeast wind events exhibit similar sea level pressure patterns. The respective magnitudes of the pressure gradients in the Lake Champlain Valley south of CYUL and the SLRV play a large role in determining the favored wind direction. Soundings of the various event types illustrate substantial differences in temperature structure, with a large near-surface temperature inversion particularly prevalent in north-northeast events. The results of this study may provide guidance in forecasting winds, temperatures, and observed weather in and around the SLRV, given certain synoptic-scale regimes.

1. Introduction

a. Motivation

Wind regimes are patterns in the observed wind field that result from the combined effects of synoptic-scale weather patterns and regional terrain surface type and topography. A prominent topographical feature of eastern Canada is the St. Lawrence River Valley (SLRV), oriented approximately southwest–northeast, extending from Lake Ontario northeastward to the Gulf of St. Lawrence (Fig. 1). Previous work identified a northeast–southwest bimodality in the wind field at multiple locations in the SLRV (Powe 1969; Cohn et al. 1996; Slonosky 2003; Carrera et al. 2009). The observed surface wind climatology at Montreal, Quebec, Canada (CYUL), shows that winds are primarily out of the north-northeast (NNE) to northeast (NE) and the west (W) to southwest (Fig. 2), corresponding to the valley's orientation in the vicinity of Montreal (Carrera et al. 2009). This directional bimodality is the manifestation of dynamically and thermally induced processes that force the wind to blow along the axis of the valley, regardless of the wind direction above ridge height (Whiteman and Doran 1993; Kossmann and Sturman 2003). Some of these processes may also be referred to as types of wind channeling.

Understanding the dynamics and the predictability of wind channeling is important for operational forecasters. Accurate wind forecasting is essential for aviation purposes; Nawri and Stewart (2006) noted that large differences between the flow within and above a valley can lead to strong turbulence. Local valley circulations also need to be well understood for proper pollution dispersion forecasting (Whiteman and Doran 1993; Kossmann and Sturman 2003), fire spread modeling and bushfire risk management (Sharples et al. 2009), cloud formation–dissolution,

* Current affiliation: Israel Meteorological Service, Bet Dagan, Israel.

Corresponding author address: Shawn M. Milrad, Dept. of Atmospheric and Oceanic Sciences, McGill University, 805 Sherbrooke Street West, Montreal, QC H3A 2K6, Canada.
E-mail: shawn.milrad@gmail.com

DOI: 10.1175/JAMC-D-11-0142.1

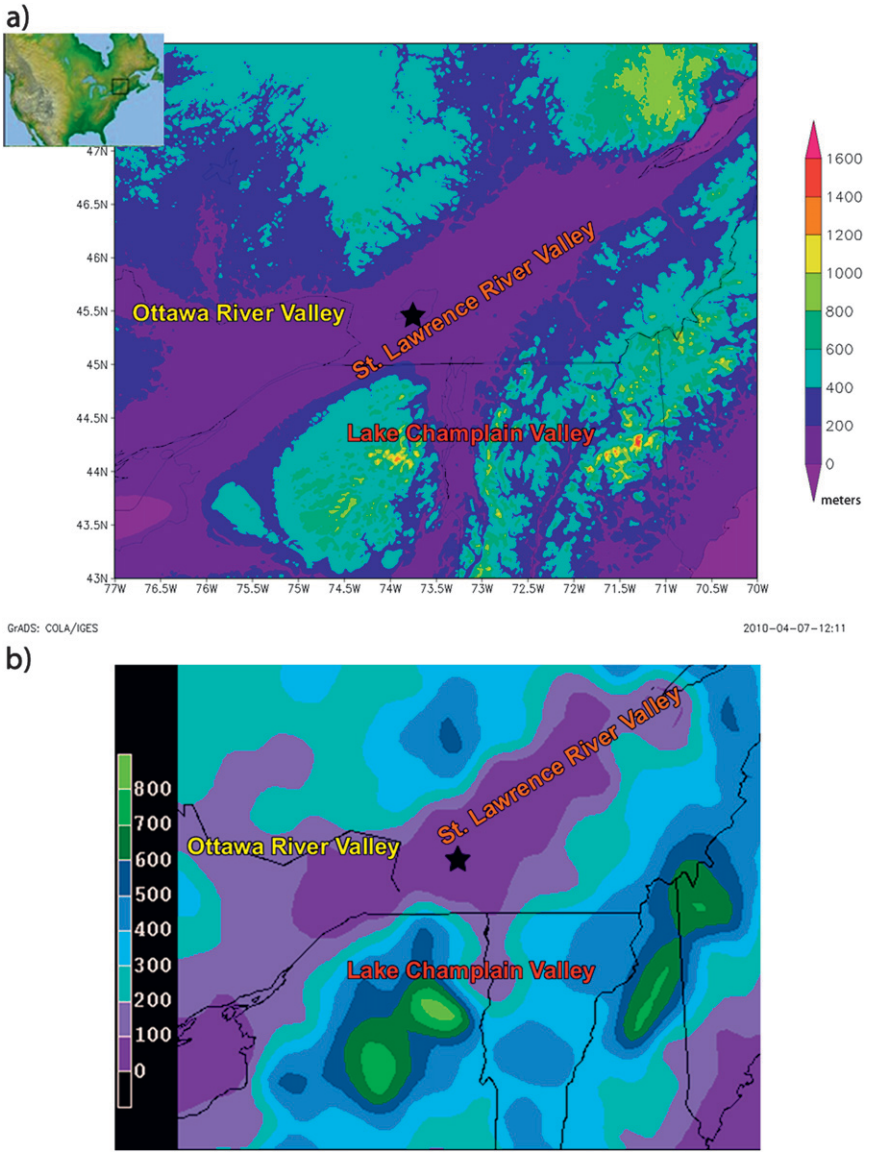

FIG. 1. Topography of SLRV in the vicinity of CYUL. (a) Elevation is plotted using the ETOP1 Global Relief Model (Amante and Eakins 2009). (b) Elevation (m) from NARR for the same geographical area shown in (a). Montreal's Trudeau International Airport is marked with a black star.

and assessing wind energy potential (Kossmann and Sturman 2003).

Wind channeling can also have a large impact on the observed weather within a particular valley region. For example, a valley may influence the formation or dissipation of deep fog (Fitzjarrald and Lala 1989) and potentially high-impact weather such as freezing rain (Ressler et al. 2012). Steenburgh et al. (1997) noted the importance of orographic channeling for near-surface temperatures and precipitation type in the Stampede Gap, a high-level mountain pass within the Cascades. Doyle and Bond (2001) documented enhanced frontogenesis resulting from a warm frontal baroclinic zone overrunning cold air channeled out of the Strait of Juan de Fuca in the Pacific Northwest.

In the SLRV, impacts of the historic January 1998 ice storm that devastated areas of northeastern North America ($3 billion of damage in Canada, over $1.4 billion in the United States; National Climatic Data Center 2008) were exacerbated by the orography of the region (Roebber and Gyakum 2003). Enhanced amounts of freezing rain fell in the SLRV, the Ottawa River Valley, and the Lake

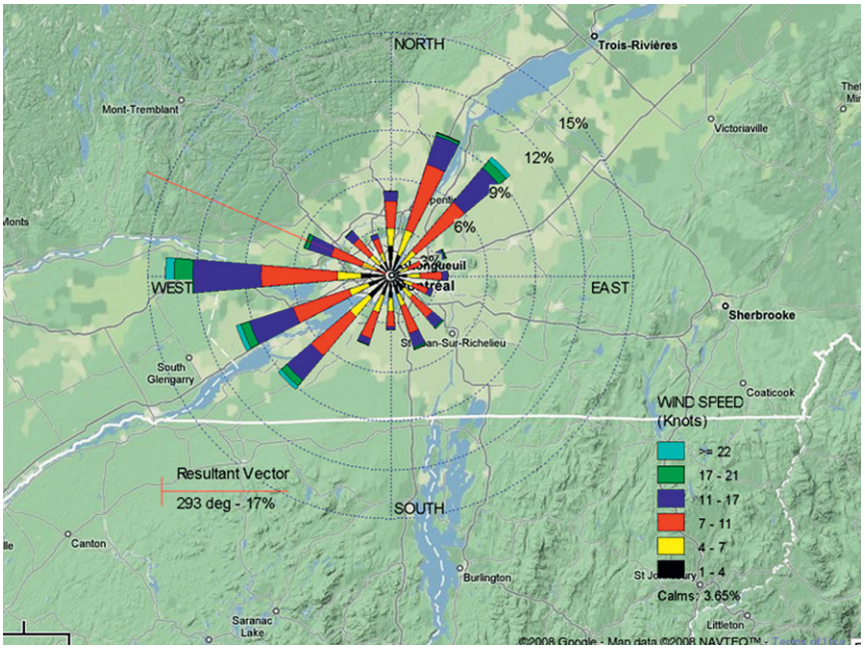

FIG. 2. Wind rose showing the climatological bimodal distribution of hourly observed surface winds at CYUL for the period 1979–2002. The background terrain map was produced using Google Maps (http://maps.google.com).

Champlain Valley (LCV). Roebber and Gyakum (2003) demonstrated that sustained, cold, orographic channeling in these valleys combined with warm southerly geostrophic flow resulted in persistent localized frontogenesis in these valleys. The channeling also helped to keep surface temperatures at or below freezing in the SLRV, so that the prolonged precipitation mainly fell as freezing rain. In the SLRV, the frontogenesis resulted from cold surface air channeled into the valley from the northeast being overrun by warm moist air advected into the region from south-southeast (SSE) synoptic-scale flow, associated with a low pressure system tracking along the Great Lakes. Furthermore, a composite analysis of 20 winter cyclones tracking through the SLRV from 1979 to 2002 revealed enhanced frontogenesis in the valley (Razy 2010). A case from, and representative of, the composite is presented in Fig. 3 and supports the frontogenesis argument of Roebber and Gyakum (2003).

b. Wind channeling conceptual review

Wind channeling in valleys has long been observed. Nearly 10 years of observations taken at Quebec City (CYQB) in the mid-eighteenth century revealed that "[b]y far the most prominent wind directions. . .were southwest (48.5%) and northeast (34.4%), reflecting the orientation of the St. Lawrence valley" (Slonosky 2003). However, it was not until the 1980s that advanced numerical simulation capabilities allowed the details of the airflow in the complex terrain to be published (e.g., Wippermann and Gross 1981; McNider and Pielke 1984; Gross and Wippermann 1987; Sturman 1987). Past work has identified four forcing mechanisms for valley winds (Whiteman and Doran 1993): thermal forcing, downward transport of momentum, forced channeling, and pressure-driven channeling.

The thermal forcing mechanism was first detailed by Jeffreys (1922). This flow is caused by temperature differences that form because of unequal surface heating and cooling rates of the valley slopes, of the valley floor, and at the same altitude in the adjacent area of noncomplex terrain (McNider and Pielke 1984). However, the thermal forcing mechanism is pertinent mainly for deep and narrow valleys (Whiteman and Doran 1993; Weber and Kaufmann 1998; Zhong et al. 2008). Because the SLRV is neither deep nor steeply sloped, Carrera et al. (2009) concluded that thermal forcing is not important in the SLRV.

The downward transport of horizontal momentum results in surface winds that are similar to the geostrophic winds aloft, and generally occurs in a neutrally stratified or unstable atmosphere (Whiteman and Doran 1993). Horizontally isotropic friction causes a decrease in wind speed, thereby decreasing the Coriolis force, which leads to a rotation of the wind by roughly 25° toward lower pressure (Whiteman and Doran 1993; Weber and Kaufmann 1998).

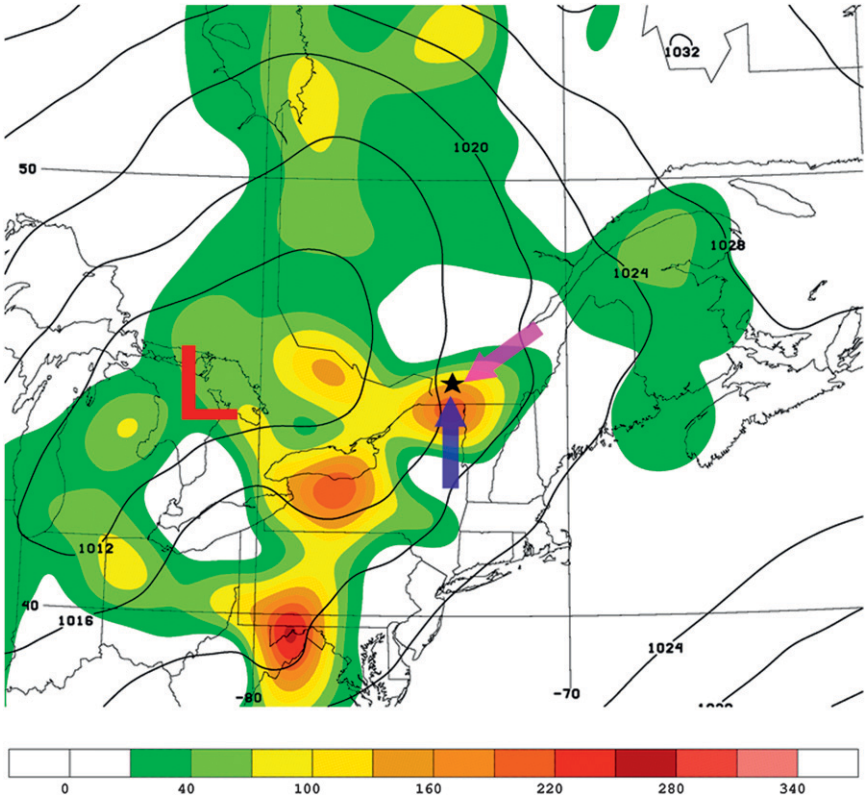

FIG. 3. Case example (1500 UTC 25 Feb 2002) of NARR near-surface frontogenesis [shaded; K (100 km)$^{-1}$ (3 h)$^{-1}$] and SLP (solid contours; hPa) in the SLRV. Schematic indicates observed valley-channeled surface wind direction (pink arrow) and approximate geostrophic wind direction (blue arrow). CYUL is marked with a black star.

This mechanism is not a channeling mechanism, as it has the same effect within or outside of a valley (Whiteman and Doran 1993). Carrera et al. (2009) identified downward momentum transport as the primary cold-season forcing mechanism at CYUL for geostrophic winds of 240°–340°.

Forced channeling also occurs when the above-valley geostrophic wind is oriented in a similar direction to the valley axis. The valley sidewalls channel the geostrophic (synoptic scale) flow with the help of anisotropic friction, which acts most strongly in the cross-valley direction (Weber and Kaufmann 1998). Originally, forced channeling was thought to be most important for narrow valleys owing to the Bernoulli effect, which dictates that the velocity of a fluid will increase as it passes through a constricted area, assuming incompressibility. However, because incompressibility is often not a valid assumption in the atmosphere, Sharp and Mass (2002) and Gabersek and Durran (2006) demonstrated that the Bernoulli effect is irrelevant to terrain-channeled winds.

The fourth mechanism, pressure-driven channeling, was simply defined by Gross and Wippermann (1987) as low-level air within a valley moving toward lower pressure (parallel to the long axis of the valley), owing to the synoptic-scale pressure gradient from one end of the valley to the other. Wippermann and Gross (1981) addressed the occurrence of this mechanism in broad and shallow river valleys such as the Rhine Valley, where channeling had previously not been expected. Further research using numerical simulations (e.g., Bergstrom and Juuso 2006) and observations (Whiteman and Doran 1993) has confirmed that wider valleys are more prone to pressure-driven channeling. Weber and Kaufmann (1998) noted that wide valleys tend to be long valleys, which may help pressure-driven channeling to develop by making it easier to form a sufficient pressure gradient between the ends of the valley (associated with the synoptic-scale pattern). It is therefore not surprising that Carrera et al. (2009) identified pressure-driven channeling as the dominant mechanism in the SLRV.

The four forcing mechanisms mentioned above are not mutually exclusive. Each forcing mechanism can dominate depending on the synoptic-scale regime, but more than one mechanism can play an important role simultaneously (Zhong et al. 2008; Schmidli et al. 2009). For

the purpose of this paper, we do not discriminate between downward momentum transport and forced channeling, since both mechanisms result in a surface wind direction similar to the geostrophic wind direction aloft. While such an exercise would be interesting, a primary focus of this study is to compare synoptic-scale regimes that are associated with pressure-driven channeling with regimes associated with forcing mechanisms wherein the surface wind is similar to the geostrophic wind aloft. Both downward momentum transport and forced channeling fall into the latter category, so both are mentioned as potential forcing mechanisms in section 4.

c. *Objectives*

Channeling is a crucial part of the wind patterns at CYUL. Considering the surrounding complex terrain, wind forecasting is challenging, especially to forecasters who are not experienced in accounting for the impacts of the local orography. However, Roebber and Gyakum (2003) suggested that there is high predictability in occurrences of synoptic-scale features coupled with the SLRV's orographic mesoscale forcing, since they are mostly controlled by large-scale pressure patterns; a mass field that is typically accurately forecasted by numerical models. Carrera et al. (2009) detailed the favored forcing (channeling) mechanisms for various types of wind events in the SLRV. This paper expands on Carrera et al. (2009) and is designed to help the local forecaster associate certain surface wind directions in the SLRV with specific synoptic-scale regimes and the associated observed weather impacts. The primary objectives of this paper are to

- partition, using manual synoptic typing, the types of prolonged NNE wind events at CYUL to provide insight into the associated synoptic-scale pressure patterns [an analysis of the geostrophic wind for each synoptic type is provided so as to elucidate the relevant forcing (channeling) mechanism],
- present an analysis of the low-level temperature structure of each synoptic type of wind event at CYUL using a composite sounding analysis [differences in vertical temperature structure (i.e., low-level lapse rates) among various synoptic types provide insight into the possible resulting observed weather at CYUL during such events (e.g., prolonged freezing rain)], and
- present a brief analysis of the associations between (i) various synoptic types of prolonged wind events and (ii) the prevalence of certain precipitation types (e.g., freezing rain versus rain).

The remainder of the paper is organized as follows: section 2 details the data used, section 3 presents the CYUL wind climatology and the case partitioning methodology, section 4 details the results of the composite synoptic and sounding analysis, and section 5 outlines conclusions and future work.

2. Data

Hourly surface data from Montreal's Trudeau International Airport were used for the cold-season months (defined for this study as December–February) from 1979 to 2002. Since this paper is a follow-up to Carrera et al. (2009), the same 1979–2002 time period was used. CYUL (Fig. 1) is located within the SLRV at an elevation of 36 m above mean sea level. The hourly temperature and 10-m wind observations were contained in the aviation routine weather report (METAR) data archive at Iowa State University, and precipitation data were obtained from Environment Canada. Histograms and wind roses were produced using MATLAB proprietary software, version 7.9.0 (Mathworks 2010). The synoptic–dynamic diagnostics were produced using the General Meteorology Package (GEMPAK), versions 5.8.3a and 5.9.4, updated from the original package devised by Koch et al. (1983).

For the synoptic-scale analysis, the National Centers for Environmental Prediction (NCEP) North American Regional Reanalysis (NARR) dataset (Mesinger et al. 2006) was used, which has a 32-km horizontal resolution, 45 vertical layers, and 3-hourly output.

Confidence in the use of NARR data for synoptic-scale analysis has already been established (e.g., Mesinger et al. 2006), and they have been used in previous wind channeling studies (e.g., Zhong et al. 2008; Carrera et al. 2009). The main limitation of NARR, when compared with hourly surface observations, is its 3-hourly time resolution. However, NARR is extremely useful for producing synoptic-scale analyses and vertical profiles that are not available from observations alone (e.g., CYUL is not an upper-air sounding station). NARR upper-level winds were compared at various times to soundings at Maniwaki, Quebec (CWMW), the closest upper-air station to the SLRV, and were found to be reliable (not shown). Moreover, NARR has provided reliable synoptic-scale and mesoscale diagnoses in the vicinity of the SLRV in a variety of recently published articles (e.g., Carrera et al. 2009; Milrad et al. 2009a, 2011; Ressler et al. 2012). A Gaussian smoothing algorithm built into GEMPAK (Koch et al. 1983) was used in this study to ensure that the geostrophic winds derived from the sea level pressure field are realistic.

Figure 1b shows that NARR topography in the vicinity of CYUL is similar to the ETOP1 topography (Amante and Eakins 2009) shown in Fig. 1a. As a result, NARR reproduces observed wind channeling with sufficient accuracy, albeit with slight discrepancies. NARR shows a relatively high frequency of east-northeast

winds in comparison with its frequency of NNE and NE winds (Figs. 4a,b). In addition, the winds are more evenly distributed between W and west-southwest (WSW) than they are in the observed wind rose (Fig. 4a). Considering that we used the observed surface winds to identify sustained NNE wind events and used NARR only for synoptic-scale analysis, these discrepancies are minor and do not affect the robustness of our results. NARR's successful representation of the bimodality in the 10-m winds (Fig. 4b) at CYUL means it is likely that it also properly replicates other terrain effects (e.g., on vertical profiles of temperature).

3. Climatology and partitioning methods used

a. CYUL wind climatology

CYUL lies at the confluence of three valleys (Figs. 1a,b). The Laurentian Mountains are located to the north of CYUL, the Adirondack Mountains to the southwest, and the Green Mountains to the southeast (SE), with the latter two also bordering the Lake Champlain Valley. All three mountain chains have individual peaks above 800 m, particularly in the Adirondacks (Fig. 1a) (Amante and Eakins 2009). While the SLRV narrows to as little as 3 km in some locations, the width is on average around 50 km and widens to roughly 90 km in the area around CYUL. The two largest (most frequent) petals in Fig. 4a are W and WSW, aligned with the broad, flat region west of CYUL where the Ottawa River merges into the St. Lawrence River. The next clear peak in a histogram of the observed wind directions at CYUL is NE and NNE (Fig. 5).

Finally, there is a smaller peak of south-southeast winds (Fig. 4a), likely due to the influence of the LCV (Powe 1969; Carrera et al. 2009). During periods of southerlies channeled northward through the LCV, the winds will wrap counterclockwise around the topography as they reach the SLRV, gaining an easterly component as they turn around the northern edge of the Adirondacks, and subsequently arrive at CYUL from the SSE. This phenomenon appears to be unique to the location of CYUL at the confluence of the three valleys. Diagnostics of observed 10-m winds elsewhere in the SRLV (e.g., Quebec City; not shown) showed NNE (NE at Quebec City) or light and variable winds during such events. SSE winds are rather uncommon at CYUL, although if present, these winds can bring warmer air into the CYUL vicinity compared to conditions in the rest of the SLRV.

The geostrophic wind climatology for Montreal (Figs. 6a,b) suggests the dominance of pressure-driven channeling in the SLRV (Carrera et al. 2009). The

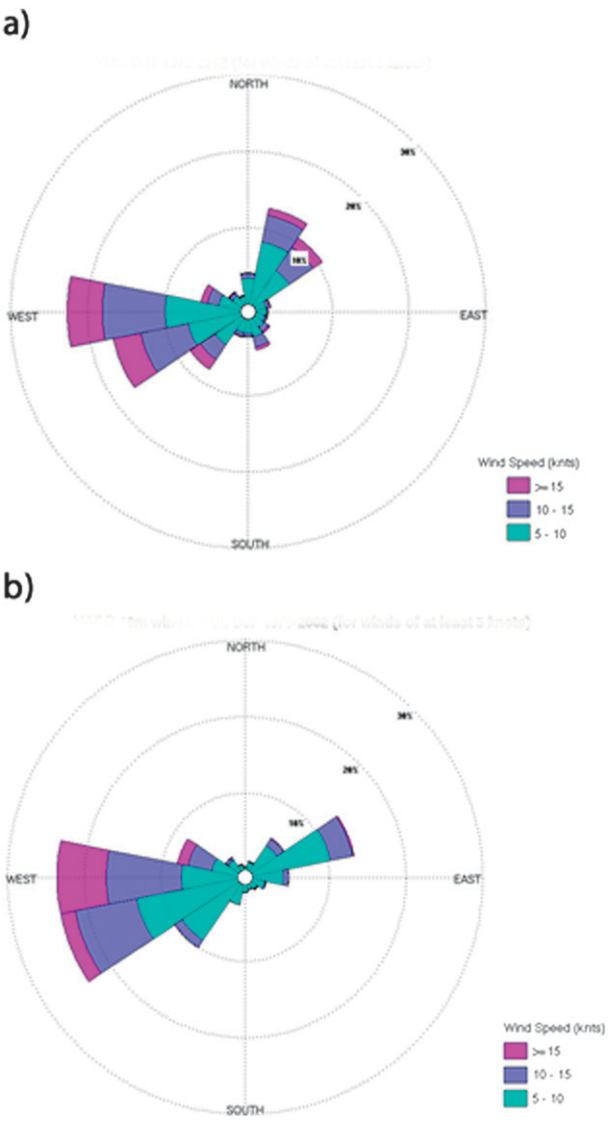

FIG. 4. Wind roses for winds of at least 5 kt during all cold-season months (December–February) from 1979 to 2002 for (a) observed winds at CYUL and (b) NARR 10-m winds interpolated to CYUL.

geostrophic winds (Figs. 6a,b) are oriented preferentially at angles perpendicular to the SLRV [SE and northwest (NW)], implying that the synoptic-scale pressure gradient is oriented parallel to the valley. If forced channeling or downward momentum transport were more important, SSE (SE) geostrophic winds would have resulted in equally prevalent SSE (SE) observed winds.

b. Synoptic partitioning methods

Manual synoptic typing is not new in atmospheric science, and has been performed for surface and upper-air analyses of weather events in west Texas (Ladd and Driscoll 1980), an environmental baseline and air quality

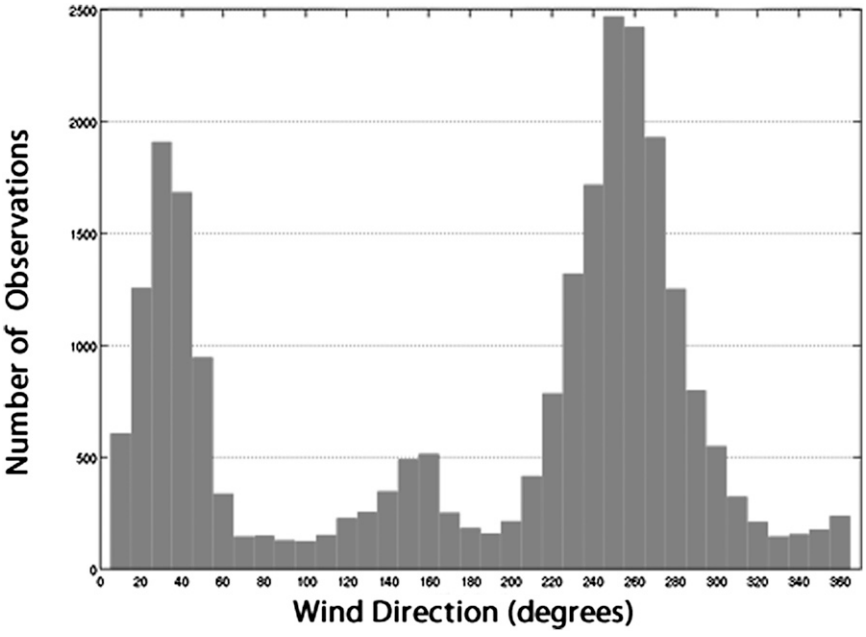

FIG. 5. Climatological wind direction histogram for cold-season (December–February) observed surface winds of at least 5 kt at CYUL from 1979 to 2002.

analysis in Louisiana (Muller 1977; Muller and Jackson 1985), and a synoptic climatology for the Gulf of Alaska (Overland and Hiester 1980). Milrad et al. (2010) used two separate manual partitioning methods to distinguish extreme precipitation events at St. John's, Newfoundland, Canada. In a study on the eastern Mediterranean, Alpert et al. (2004) found automated typing methods to be unsuccessful. They suggested that manual typing might be preferable to more automated techniques when dealing with phenomena impacted by the local topography, since "[l]ocal weather phenomena. . .are very sensitive to minor differences in the route or location of the synoptic systems in conjunction with the complex (Eastern Mediterranean) topography."

The application of a manual synoptic typing method for wind channeling events at CYUL allows for the diagnosis of favored synoptic-scale regimes for sustained wind events. The results may enhance the ability of the local forecaster to anticipate sustained wind events and associated observed weather impacts at CYUL by simply identifying the synoptic-scale pattern, based on the results in section 4.

Here, wind events were determined solely by hourly wind observations at CYUL. Three groups of wind events were established, corresponding to the most preferred wind directions at CYUL: WSW, NNE, and SSE. Although WSW events are most prevalent in the climatology, these events are primarily associated with positive pressure tendencies and fair weather, and therefore are far less associated with hazardous precipitation (Razy 2010). Thus, the synoptic–dynamic analysis in section 4 focuses only on NNE and SSE events.

An NNE wind event is defined as one in which the CYUL wind direction is 10°–50°, inclusive, for at least 12 consecutive hours with a minimum speed of 5 kt (1 kt $\simeq$ 0.5 m s^{-1}) throughout. An SSE wind event is one in which the wind at CYUL is 140°–160°, inclusive, with identical speed and duration requirements. These ranges were chosen because they contained the highest number of observations in the climatology (Fig. 5). The 5-kt threshold was chosen to ensure that the winds are driven by the synoptic-scale pattern, as light and variable winds are normally caused by subsynoptic-scale processes (i.e., turbulent eddies). The minimum duration was also chosen to ensure that the channeling was at least in part forced by synoptic-scale processes, which tend to occur on time scales longer than a few hours. To ensure synoptic-scale event independence, there must have been at least 48 h between events. If two events met the minimum duration requirement but were separated, for example, by 24 h, neither event was counted.

Using the above criteria, we found 171 synoptically independent NNE wind events and 16 synoptically independent SSE wind events. In our experience and in previous papers that produced synoptic-scale composites (e.g., Sisson and Gyakum 2004; Milrad et al. 2009b), having two groups with vastly different numbers of cases is not advisable. Thus, to simplify the analysis, the number of NNE events was reduced by calculating the median (e.g., Sisson and Gyakum 2004; Milrad et al. 2009b)

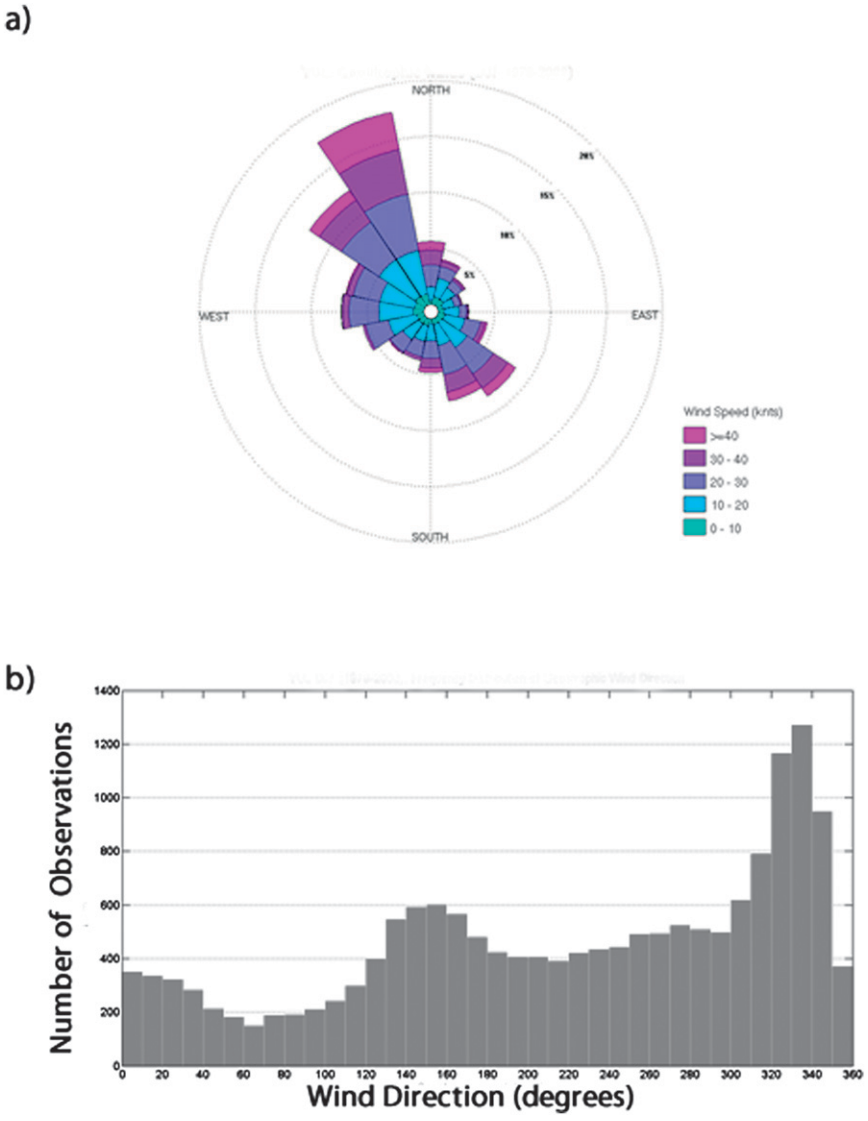

FIG. 6. Climatological (a) wind rose and (b) wind direction histogram for NARR cold-season (December–February) geostrophic winds based on MSLP and interpolated to CYUL, 1979–2002.

duration of these events, 19 h. To narrow our study to approximately 50 NNE events—a number used by Sisson and Gyakum (2004) and Milrad et al. (2009b)—only NNE events that lasted 19 ± 3 h were considered. In all, 55 NNE and 16 SSE events were used for synoptic-scale compositing. For reference, the date and time of each NNE and SSE event used in this study are given in the appendix in Tables A1 and A2, respectively.

1) PARTITIONING NNE WIND EVENTS

The composite mean sea level pressure (MSLP) analysis for all 55 NNE events shows very weak features that are consistent with large amounts of composite smearing (Fig. 7a). Additionally, Fig. 7b shows that there is substantial variability in the geostrophic winds at CYUL during NNE wind events, suggestive of multiple sea level pressure patterns responsible for NNE events. We employed a manual synoptic typing procedure to further partition the NNE events (described later in this section). Though smeared, the composite MSLP plot in Fig. 7a does suggest pressure-driven channeling, with relatively high pressure at the northeastern end of the SLRV, and relatively low pressure toward the southwest. The pressure gradient force is clearly pointing toward the southwest along the axis of the valley. The suggestion of pressure-driven channeling during NNE

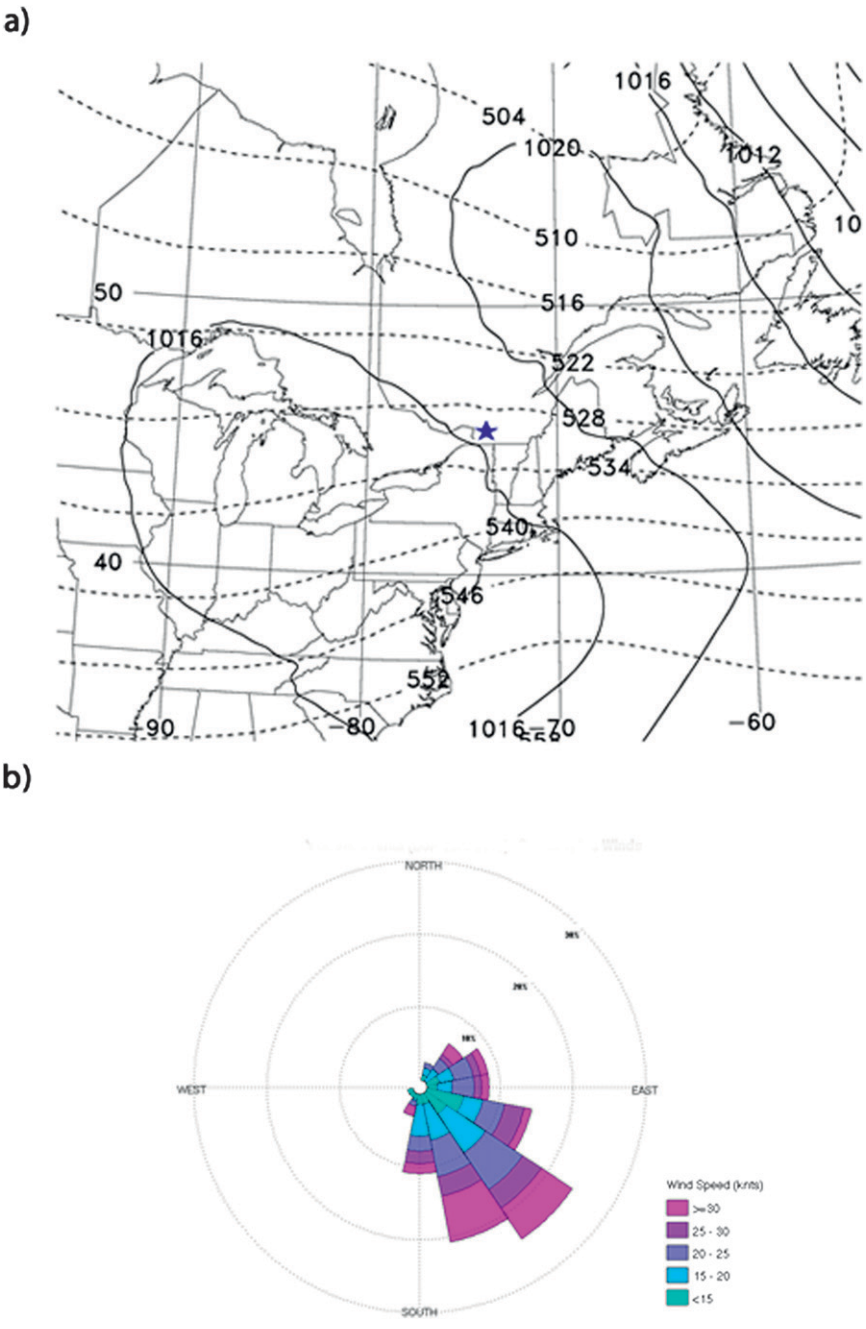

FIG. 7. NARR (a) composite of MSLP (hPa; solid lines) and 1000–500-hPa thickness (m; dashed lines) and (b) wind rose of geostrophic wind based on MSLP, for all 55 NNE wind events at CYUL, marked with a blue star.

events is supported by the dominance of SE geostrophic flow during NNE observed events (Fig. 7b). Forced channeling or downward momentum transport would be associated with primarily NNE geostrophic winds.

The use of manual synoptic typing to partition NNE wind events into physically distinct groups is informed by our knowledge of the meteorology of the region as opposed to more purely mathematical or statistical methods (Alpert et al. 2004). The method used was made as objective as possible so as to make the results reproducible, with "borderline" cases rejected. We utilized the deviation from the area-averaged MSLP over 40°–55°N and 60°–90°W (approximately 1650 km × 2250 km),

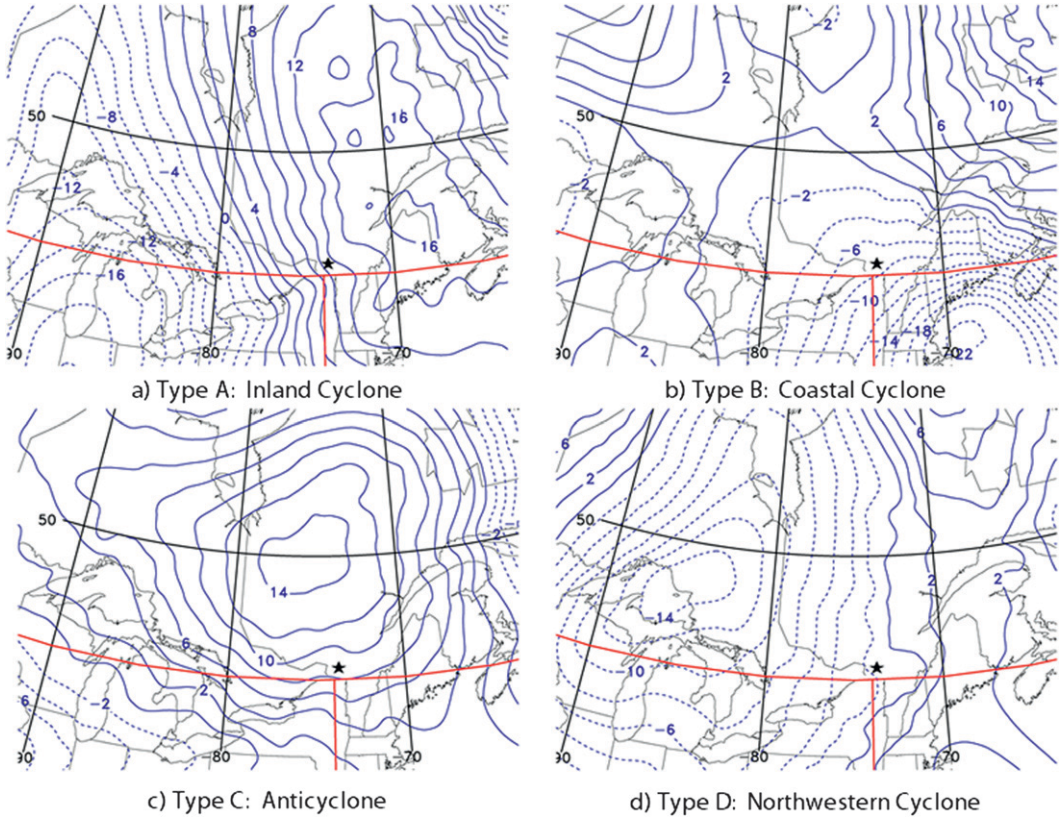

FIG. 8. Examples of MSLP deviation maps for each of the four synoptic types of observed NNE wind events: (a) type A (inland cyclone), 0300 UTC 12 Dec 1983, (b) type B (coastal cyclone), 0300 UTC 8 Feb 1983, (c) type C (anticyclone), 1800 UTC 4 Jan 1998, and (d) type D (northwestern cyclone), 2100 UTC 23 Dec 2001. Solid lines denote positive pressure deviations and dashed lines denote negative pressure deviations (hPa). CYUL is marked with a black star and the red lines denote the boundaries for delineating among types A, B, and D.

which is representative of approximately one-half of a synoptic-scale wavelength. This was desirable because (i) it is sufficiently large to successfully capture synoptic-scale pressure systems and (ii) it remains sufficiently small so that pressure systems far removed from the SLRV do not impact the areal average. Because the goal of this partitioning is to identify different synoptic patterns leading to NNE events, the technique must be able to discern between different synoptic features that commonly affect the CYUL region. Relatively high pressure to the north is associated with anticyclones that are located over northeastern Quebec or farther east over the Atlantic Ocean. However, low pressure systems south of CYUL are expected to be associated with one of *three* predominant storm tracks: two inland cyclone tracks, one north and one south of the Great Lakes, and a coastal cyclone track, whereby lows move northward along the New England coast. To distinguish among the three low pressure tracks, borders are drawn along the 74°W longitude line (vertical red line in Fig. 8), the nearest whole degree of longitude at CYUL (73.74°W), and along the 45°N latitude line (horizontal red line in Fig. 8), which is the nearest whole degree of latitude at CYUL (45.4°N). The manual synoptic partitioning of NNE wind events worked as follows:

- The middle time step (rounded to the nearest 3-hourly time step, to correspond with NARR data) of each NNE wind event was selected.
- The deviation from the area-averaged value of MSLP in the box described above was calculated at each grid point within that box. Grid points in NARR are located every 32 km.
- The features with the strongest anomalies were identified (e.g., Fig. 8). These anomalies are expected to correspond to high pressure systems located at latitudes north of CYUL, and low pressure systems located either to the southeast, southwest, or northwest of CYUL.

Four types of NNE events were identified using the manual synoptic typing, and a case example of each is presented in Fig. 8: (i) type A: inland cyclone (Fig. 8a), in which the negative pressure deviation is west of 74°W

TABLE 1. The number of events in each synoptic type of NNE wind event ($n = 55$).

Type	Type A: inland cyclone	Type B: coastal cyclone	Type C: anticyclone	Type D: northwestern cyclone
No. of events	33	11	6	5

and south of 45°N; (ii) type B: coastal cyclone (Fig. 8b), in which the negative pressure deviation is east of 74°W and south of 45°N; (iii) type C: anticyclone (Fig. 8c), which has no negative pressure deviation within half a synoptic wavelength of CYUL; and (iv) type D: northwestern cyclone (Fig. 8d), in which the negative pressure deviation is west of 74°W and north of 45°N. The number of cases in each group is in Table 1 and the synoptic structures associated with each type of event will be discussed in detail in section 4.

2) PARTITIONING SSE WIND EVENTS

Unlike for NNE wind events (Fig. 7b), the geostrophic wind rose for SSE wind events shows little directional variability (Fig. 10b), which is highly suggestive of similar sea level pressure patterns during each SSE wind event. Moreover, a case-by-case examination of the sea level pressure field associated with the 16 SSE events revealed similar synoptic-scale structures. Therefore, we treated the 16 SSE events as one group of events, with no need for further partitioning. The synoptic-scale structures associated with SSE events are discussed in section 4.

4. Composite synoptic-scale analysis

a. Large-scale patterns

For the discussion of vertical motion in this section, we utilize the adiabatic, frictionless form of the quasigeostrophic (QG) omega equation (Bluestein 1992, p. 328):

$$\left(\nabla_p^2 + \frac{f_o^z}{\sigma}\frac{\partial^z}{\partial p^z}\right)\omega = -\frac{f_o}{\sigma}\frac{\partial}{\partial p}[-\mathbf{v}_g \cdot \nabla_p(\zeta_g + f)] + \frac{R}{\sigma p}[-\nabla_p^2(-\mathbf{v}_g \cdot \nabla_p T)], \quad (1)$$

where f and σ are the Coriolis and static stability parameters, ζ_g and $\mathbf{v}_g$ are the geostrophic relative vorticity and the geostrophic wind, R is the gas constant, p is pressure, and T is temperature. The two terms on the right-hand side are differential vorticity advection and the Laplacian of horizontal temperature advection, wherein cyclonic vorticity advection (CVA) increasing with height and spatial gradients of horizontal warm-air advection (WAA) are associated with the QG-generated ascent of air. It is assumed that vorticity advection at low levels is small compared to the midtroposphere, so that 500-hPa CVA is associated with the QG-generated ascent of air.

1) NNE WIND EVENTS

Figure 9 shows the composite NARR MSLP and 1000–500-hPa thickness patterns for each NNE wind event type. The composite is produced using the middle time step of each event. Type A (inland cyclone) (Fig. 9a) is the largest group of NNE events ($n = 33$) and therefore still shows relatively weak features in the composite MSLP pattern, indicative of some case-to-case variability in the location of the individual features. However, these features are more well-defined than they are in the overall NNE event composite (Fig. 7a), showing the utility of the partitioning scheme. A composite anticyclone is present over northeastern Quebec at the eastern end of the SLRV, and a composite cyclone is present at the western end of the SLRV. The isobars are perpendicular to the SLRV, suggestive of pressure-driven channeling with geostrophic winds primarily from SE and SSE (Fig. 9b). Powe (1969) found that this setup is the most common for observed NNE winds at CYUL. This result has substantial observed weather impacts in that cold near-surface air can remain in place despite warming temperatures aloft (e.g., geostrophic WAA is evident in Fig. 9a). Extreme cases of the setup present in Fig. 9a feature a strong low-level temperature inversion (section 4b) and can lead to prolonged periods of freezing precipitation, as in the 1998 ice storm (Gyakum and Roebber 2001; Roebber and Gyakum 2003). Finally, both CVA and lower-tropospheric WAA are present at CYUL during these events, indicating unambiguous QG-generated ascent of air [Eq. (1)].

The type B ($n = 11$) (coastal cyclone) composite is presented in Fig. 9c. A weak composite anticyclone is located in northern Quebec, with a 1004-hPa composite cyclone located off the coast of New Jersey. The geostrophic winds primarily have an easterly component (Fig. 9d) and a substantial percentage of the geostrophic winds (50%) are east-northeast or NE, roughly parallel to the long axis of the SLRV. This is suggestive of either the forced channeling or downward momentum transport mechanism (or both), in which the surface winds are in a direction similar to the geostrophic winds. While our results show that forced channeling or downward momentum transport is only evident in a small percentage (one-half of type B, etc.) of our total NNE events, it is

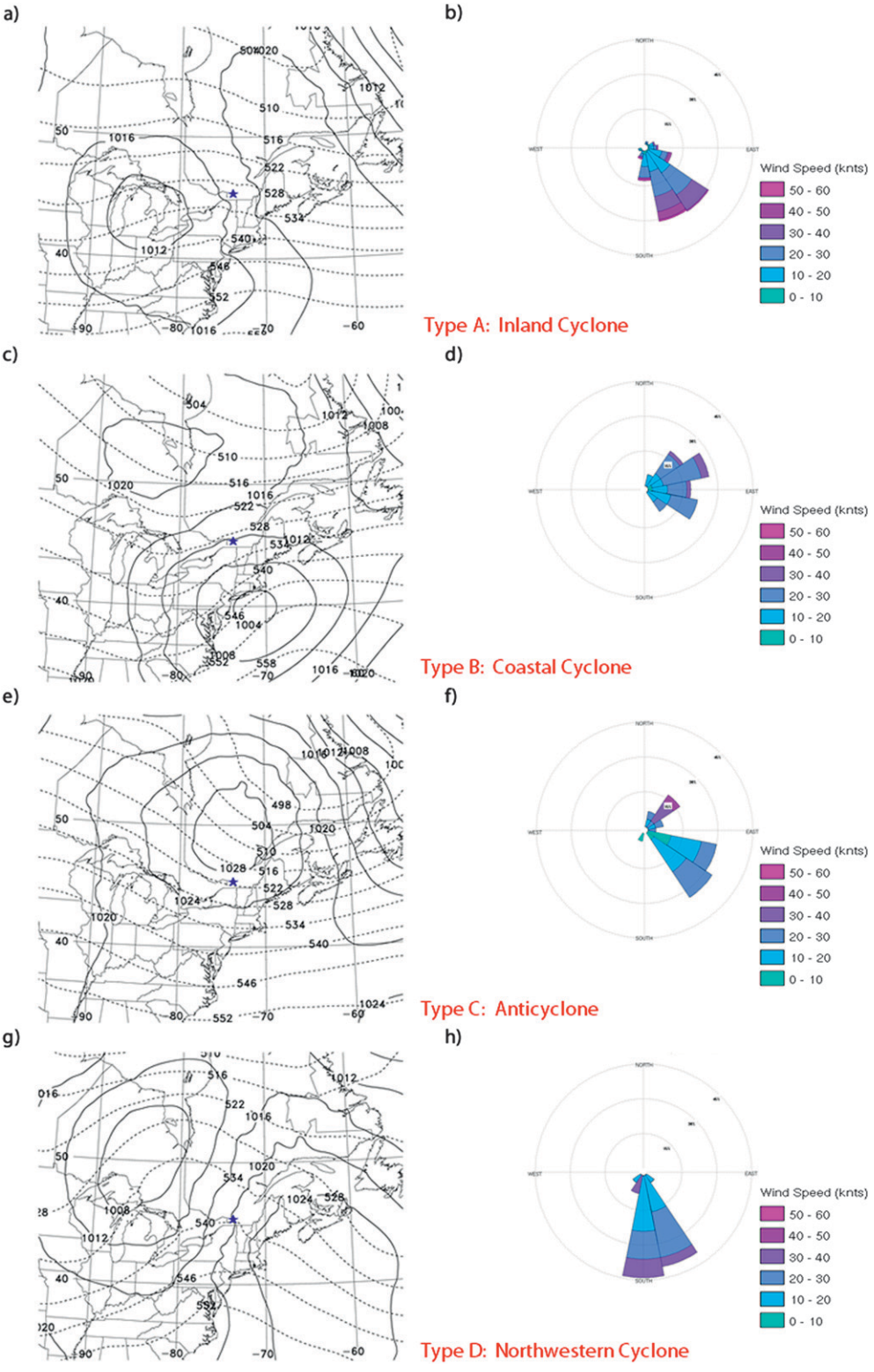

FIG. 9. (left) Composites of MSLP (solid lines; hPa) and 1000–500-hPa thickness (dashed lines; m) for the four types of NNE wind events at CYUL, marked with a blue star. (right) The corresponding geostrophic wind roses for MSLP data interpolated to CYUL. (a),(b) Type A (inland cyclone, $n = 33$), (c),(d) type B (coastal cyclone, $n = 11$), (e),(f) type C (anticyclone, $n = 6$), and (g),(h) type D (northwestern cyclone, $n = 5$).

nonnegligible. Some type-B events (40%) do result in pressure-driven channeling, as exhibited by the SE geostrophic winds at CYUL in Fig. 9d. The composite 1000–500-hPa thickness pattern indicates an upper-level trough to the west of the composite cyclone. This implies that CVA [Eq. (1)] is the main mechanism for the QG-generated ascent of air at CYUL in type B, given the absence of WAA in Fig. 9c. This stands in contrast to the prevalence of both CVA and WAA in type-A events (Fig. 9a).

The third type of NNE events, type C (anticyclone), is the only one where a composite cyclone is not present within the vicinity of the SLRV (Fig. 9e). The pattern is dominated by a 1028-hPa composite anticyclone centered near Quebec City (Fig. 9e). The composite pressure gradient is oriented parallel to the SLRV, suggesting that pressure-driven channeling is the dominant mechanism. This is strongly supported by primarily SE geostrophic winds at CYUL (Fig. 9f). However, in a small subset of cases, the surface anticyclone is located farther to the north than in the composite (Fig. 9e), resulting in NE geostrophic winds. Thus, while most occurrences of type C result in pressure-driven channeling, a few are likely associated with forced channeling or downward momentum transport. CYUL is clearly located downstream of a composite upper-level ridge, implying anticyclonic vorticity advection (AVA) at CYUL (Fig. 9e). In combination with the slight cold-air advection (CAA) evident in Fig. 9e, it is highly likely that type-C events are not associated with heavy precipitation events at CYUL, since both AVA and CAA are suggestive of the QG-generated descent of air [Eq. (1)].

The type-D (northwestern cyclone) composite is shown in Fig. 9g. While this type has the fewest number of cases ($n = 5$), the associated synoptic-scale structures provide important physical insight. In Fig. 9g, a composite cyclone is located north of Lake Huron, while a composite anticyclone is centered off the coast of New England. The resulting geostrophic winds at CYUL are predominantly southerly and south-southwesterly (SSW) (Fig. 9h). While one might expect this regime to result in forced southerly channeling northward through the LCV and into CYUL, the NNE to SSW pressure gradient along the SLRV is strong enough to produce pressure-driven channeling and NNE-observed winds at CYUL. As in type A, this finding is important in terms of vertical temperature profiles and observed weather, as prolonged NNE surface winds tend to be associated with large temperature inversions and prolonged freezing precipitation at CYUL, which will be further discussed in section 4b. The primary QG mechanism for ascent in type-D events appears to be geostrophic WAA (Fig. 9g). In the next section, we will compare and contrast type D and the SSE wind event composite, which at first sight have very similar MSLP patterns.

2) SSE WIND EVENTS

During SSE events ($n = 16$), a composite cyclone is located over northeastern Ontario, Canada, and northwestern Quebec (Fig. 10a). A composite anticyclone is centered over the Atlantic Ocean southeast of Nova Scotia, Canada. Compared to the overall NNE event composite (Fig. 7b), the prevalence of geostrophic winds of 30 kt or greater is higher in the SSE event composite (Fig. 10b). This suggests a stronger synoptic-scale pressure gradient in SSE events than in NNE events. Additionally, the directional range of geostrophic winds is more limited than for NNE events. Approximately 50% of the geostrophic winds are south-southwest, and the remainder is split between south and southwest. There is a distinct lack of SSE geostrophic winds, contrasting with the presence of NNE geostrophic winds during some observed NNE events (Fig. 7b). In particular, the presence of SSW geostrophic winds during SSE wind events suggests that sometimes, neither the forced channeling nor the downward momentum transport mechanisms are at play, since they would result in observed winds at CYUL out of the SSW or south. While Carrera et al. (2009) found that forced channeling is dominant in the LCV, the MSLP pattern in Fig. 10a suggests that pressure-driven channeling in the LCV is likely responsible for some SSE wind events at CYUL, with the pressure gradient force pointing approximately from SE to NW.

The composite MSLP and 1000–500-hPa thickness patterns in the SSE event composite (Fig. 10a) are remarkably similar to those observed in type-D NNE events (Fig. 9g). Thus, it is important to the operational forecaster that the differences between these two patterns be illuminated, since they result in substantially different observed weather. In general, NNE winds keep low-level cold air entrenched in the valley, while SSE winds advect warm air from the south.

The along-SLRV component of the synoptic-scale pressure gradient force is weaker for SSE events than for type-D NNE events (not shown). Therefore, it is easier for the channeled winds from the LCV to overwhelm the NNE pressure-driven channeling during SSE events. Another critical issue is the strength of the channeling within the LCV. Figure 10a suggests that *both* forced channeling (or downward momentum transport) and pressure-driven channeling may be causing southerlies in the LCV (with low pressure to the north). To further examine the role of pressure-driven channeling in the LCV during type-D NNE and SSE events, the pressure

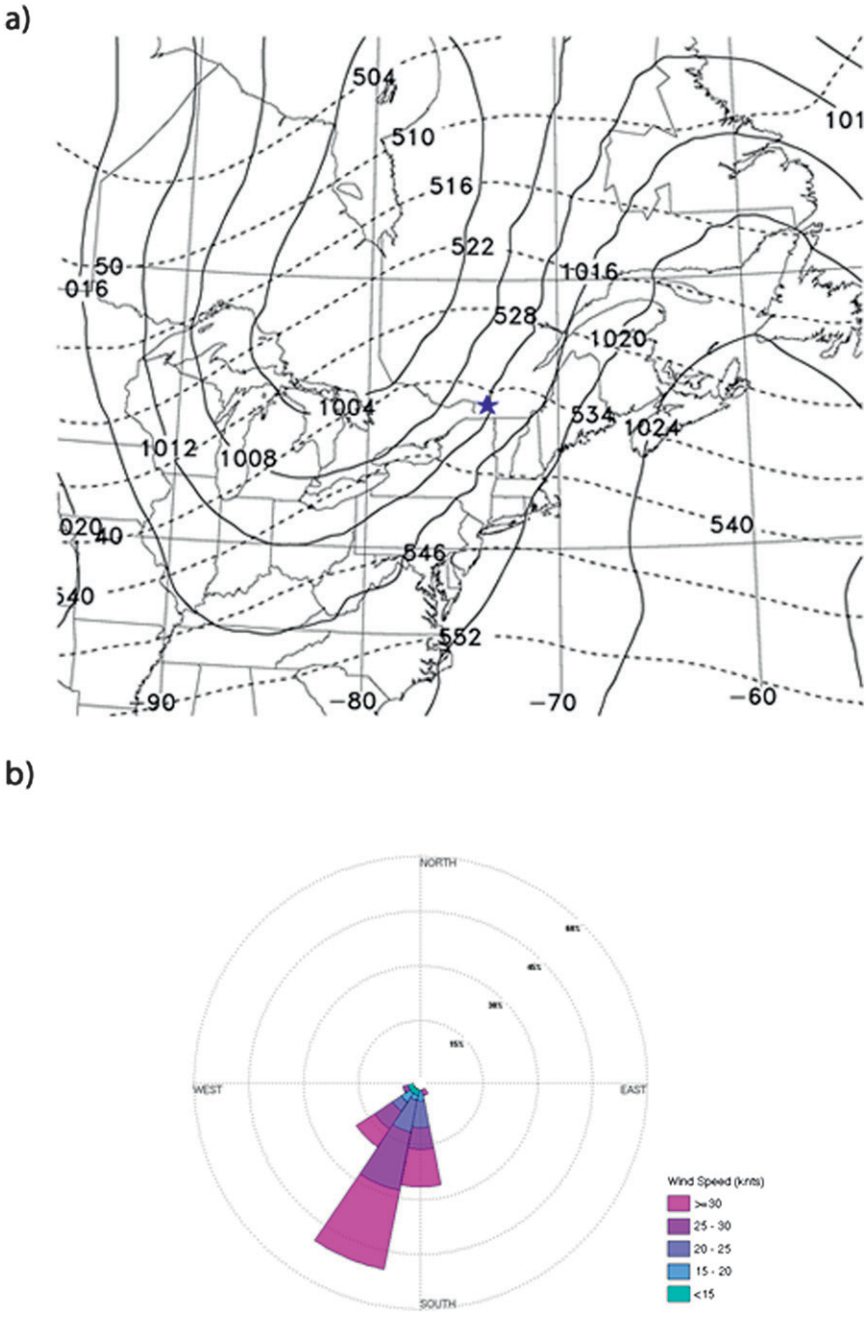

FIG. 10. Composite of all 16 SSE wind events at CYUL. (a) MSLP (solid lines; hPa) and 1000–500-hPa thickness (dashed lines; m) for SSE wind events at CYUL, marked with a blue star, and (b) the geostrophic wind rose.

gradient in the LCV was calculated for each event, at the NARR time step closest to the middle of the event. The MSLP difference was calculated between CYUL (located at the northern end of the LCV; elevation: 36 m) and Albany, New York (KALB; 42.76°N, 73.80°W; located at the southern end of the LCV; elevation: 92 m), and the results are displayed in Fig. 11. For over 80% of SSE events, the pressure gradient in the LCV is stronger than in all five type-D NNE events. Thus, we hypothesize that given a low pressure system northwest of CYUL, sustained SSE winds will most likely occur at CYUL if the pressure gradient along the SLRV is relatively weak in combination with a particularly strong pressure gradient along the LCV. Such a set of relatively

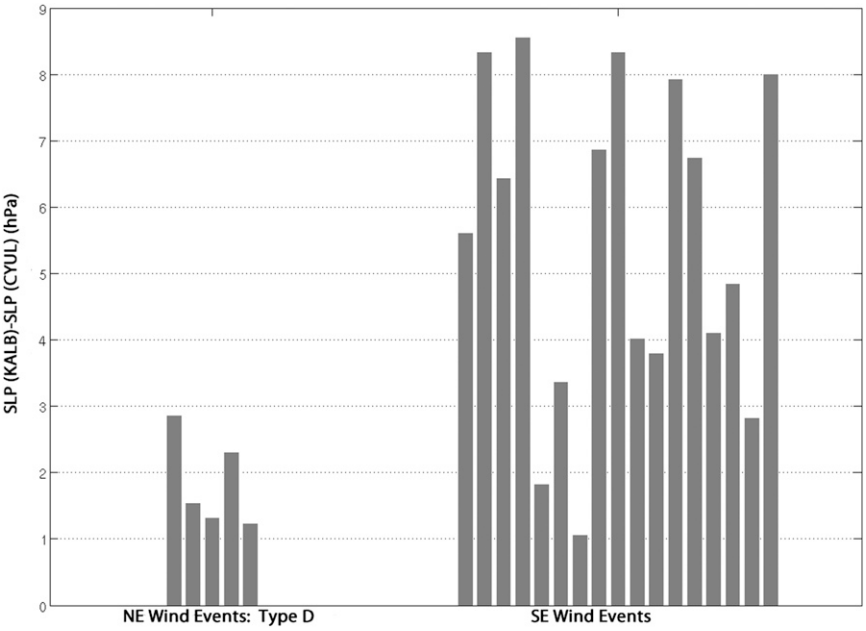

FIG. 11. Bar graph of the pressure gradient (hPa) along LCV between KALB to the south and CYUL to the north during (left) type-D (northwestern cyclone) NNE wind events and (right) all SSE wind events at CYUL. Positive differences signify a northward-pointing pressure gradient force.

stringent conditions elucidates why SSE events are relatively uncommon at CYUL.

b. Soundings

Composite NARR soundings for each of the NNE wind event types and the SSE events were produced to illustrate differences in the vertical temperature structures, with a particular focus on assessing low-level stability. To produce composite soundings, all NARR time steps during a wind event were included, except those between 0600 and 1500 UTC, inclusive, so as to avoid bias due to typical nocturnal low-level stability. Some NNE wind events may involve nocturnal low-level stability owing to reasons other than radiational cooling (such as the pressure-driven channeling itself), but such an assessment is left for future work. Figure 12 shows vertical profiles of NNE events for types A, B, and C, respectively. The veering wind profile in Fig. 12a supports the earlier assertion of strong WAA at CYUL in type A. In contrast, temperature advection is essentially negligible in types B and C (Figs. 12b,c), as the wind shift in the 900–800-hPa layer appears to be due to a discontinuity between the boundary layer and the free atmosphere. Type B (Fig. 12b) is the most saturated type, particularly in the lowest 100 hPa, suggestive of the relatively moist air being advected from the Atlantic Ocean (Fig. 9c). Type C (Fig. 12c) is the driest, and this type is the least associated with precipitation at CYUL, as only 25% of the total event hours are associated with precipitation (Table 2).

Both types B and C (Figs. 12b,c) have elevated temperature inversions in contrast to type A (Fig. 12a), which exhibits a large near-surface temperature inversion. This illustrates why, relative to types B and C in Fig. 12, type A would be most commonly associated with freezing rain and drizzle at CYUL: it is difficult to form freezing rain or drizzle without a large surface-based temperature inversion. In fact, 16% of all precipitation reports during type-A events are freezing rain or drizzle, compared to 5% and 4% for types B and C, respectively (Table 2).

In section 4a, type-D NNE events and SSE events were shown to have similar composite MSLP and thickness patterns. Figure 13 compares the composite vertical profiles of these two groups. The SSE composite shows that the troposphere is generally closer to saturation than in type D (Fig. 13). In addition, the mean temperatures at and just above the surface (approximately the lowest 30 hPa) are considerably warmer for SSE events. As shown in Table 2, this finding is consistent with a much smaller likelihood of liquid precipitation occurring in NNE events than in SSE events. Of all reported hours of precipitation for type-D events, 48% are freezing rain or freezing drizzle, while only 2%

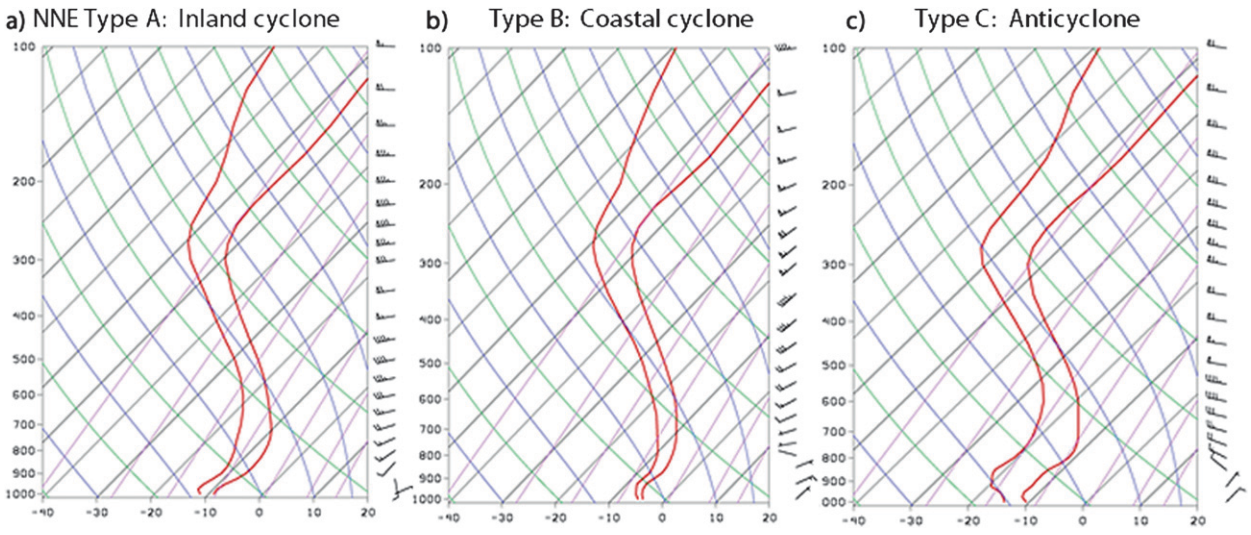

FIG. 12. NARR composite vertical profiles of temperature and dewpoint temperature (°C), and wind (barbs) at Montreal for three of four types of NNE wind events: (a) type A (inland cyclone), (b) type B (coastal cyclone), and (c) type C (anticyclone). Data were used from each NARR time step during a wind event, except for 0600–1500 UTC, inclusive, to avoid biasing due to nocturnal low-level stability.

are such for SSE events. Moreover, liquid precipitation is never observed during any type-D NNE wind event, yet it accounts for nearly half of the total precipitation hours in SSE cases (Table 2).

There is a difference in the strength of the low-level (lowest 100 hPa) temperature inversion between SSE events and type-D events (Fig. 13). In type-D events, cold air is funneled along the SLRV via near-surface NNE winds (Fig. 13). In the SSE events, the warmer LCV air is transported into CYUL via SSE near-surface winds. The steep inversion evident in type D (Fig. 13) is similar to that of type A (Fig. 12a) and is particularly well suited to producing freezing rain or drizzle (Table 2), given the appropriate surface temperatures. The deep isothermal layer in SSE events (Fig. 13), however, would preserve the phase of hydrometeors falling into that layer until they reach the surface, so that they either melt and stay melted, or remain frozen as they fall.

The veering wind profile indicates WAA in the lowest layer of the atmosphere during SSE events (Fig. 13), which results in a well-mixed, isothermal lower troposphere. In contrast, the boundary layer is decoupled from the free atmosphere in type-D events (Fig. 13) (in association with the temperature inversion), relegating the WAA to a layer above the surface (Fig. 13). This helps to create a steep inversion for type-D events, supporting the association of this type with freezing precipitation.

5. Concluding discussion and future work

Wind channeling in the SLRV is an important contributor to the observed weather patterns in and around Montreal, Quebec (CYUL), which can have a large impact on life and property. Pressure-driven channeling, where the wind blows from high to low pressure along

TABLE 2. The frequency of precipitation, freezing precipitation (freezing rain and drizzle), and liquid precipitation observations for each NNE wind event type and all SSE wind events. The total number of event hours is the sum of the hourly duration of each wind event.

Type	NNE type A: inland cyclone	NNE type B: coastal cyclone	NNE type C: anticyclone	NNE type D: northwestern cyclone	SSE events
No. of events	33	11	6	5	16
Sum total of event hours	622	233	110	87	251
% of total event hours that reported precipitation	53	41	25	29	46
% of total precipitation event hours that reported freezing precipitation	16	5	4	48	2
% of total precipitation event hours that reported liquid precipitation	4	13	0	0	44

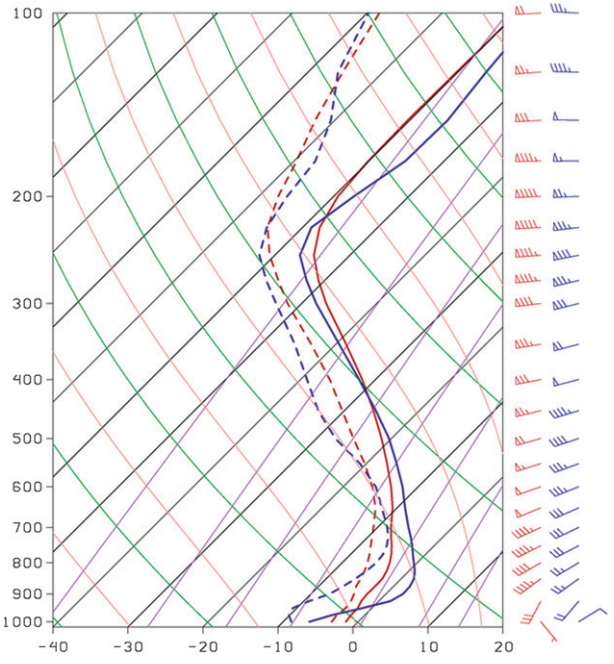

FIG. 13. NARR composite vertical profiles of temperature (°C; solid lines), dewpoint temperature (°C; dashed lines), and winds (kt; barbs) at Montreal for SSE wind events (red lines) and type-D (northwestern cyclone) NNE wind events (blue lines).

the axis of the valley, is shown to be the predominant mechanism for 55 NNE wind events at CYUL, with forced channeling and downward momentum transport (both resulting in flow approximately parallel to the geostrophic wind) identified as secondary mechanisms. Both pressure-driven channeling and either forced channeling or downward momentum transport are identified as forcing mechanisms for the 16 SSE wind events at CYUL.

This paper associates various types of wind events with particular synoptic-scale pressure patterns. NNE events were partitioned into four synoptic types, using manual synoptic typing based on area-averaged MSLP deviations. Type A (inland cyclone; Fig. 9a) ($n = 33$) features a composite cyclone tracking over the Great Lakes and a composite anticyclone in northeastern Quebec. Pressure-driven channeling from NNE winds results in the near-surface layer remaining substantially colder than air aloft, despite geostrophic WAA, and a large temperature inversion results (Fig. 12a). Type B (coastal cyclone) involves a composite cyclone east of New Jersey and a composite anticyclone over northern Quebec and is associated with CVA (Fig. 9c) as a QG mechanism for the ascent of air. This type also features a more moist air column (Fig. 12b), consistent with geostrophic flow from the Atlantic Ocean. Type C (anticyclone) is the only type without a composite cyclone present and is dominated by a strong anticyclone in northeastern Quebec (Fig. 9e). Accordingly, both AVA and weak CAA are present at CYUL and this type is the driest of all NNE wind event types (Fig. 12c). Type D (northwestern cyclone) events, which occur infrequently ($n = 5$) compared to the other types, have a composite cyclone located north of Lake Huron, while a composite anticyclone is centered off the coast of New England (Fig. 9g). Despite the southerly geostrophic flow, the pressure gradient force along the SLRV is strong enough to result in pressure-driven channeling from the northeast. As in type A, a large near-surface temperature inversion (Fig. 13) is present despite geostrophic WAA (Fig. 9g).

Type-D NNE events and all 16 SSE events exhibit similar composite MSLP and 1000–500-hPa thickness patterns (Figs. 9g, 10a), despite different surface wind directions. For winds to be SSE at CYUL, the pressure gradient along the LCV to the south of CYUL must be relatively strong, and the pressure gradient along the SLRV must be relatively weak (Fig. 11). In contrast, type-D NNE events feature a relatively weak pressure gradient along the LCV and a strong pressure gradient along the SLRV, which allows NNE surface winds to dominate. This finding has crucial importance to forecasters, as the two resulting vertical profiles are different (Fig. 13). The SSE wind composite shows a well-mixed isothermal layer in the lower troposphere while type-D events exhibit an extremely strong temperature inversion (Fig. 13). This suggests that hazardous conditions such as freezing rain are much more likely in type-D events (Table 2), despite only subtle differences in the synoptic-scale pattern.

This paper highlights some of the forecasting issues associated with orographic wind channeling in the SLRV, and may help the local forecaster to associate certain synoptic-scale regimes with the resulting wind direction and observed weather patterns around CYUL. Specifically, given an accurate prediction of the SLP field from a numerical model, the forecaster can use the results of this paper to assist with manual pattern recognition, in order to associate the predicted SLP pattern with the local surface winds at CYUL (which a forecast model might not correctly predict because of insufficient horizontal resolution, etc.). In a future paper, we will more specifically address (i) temperature trends and (ii) precipitation statistics, including frequency, amount, and precipitation types associated with NNE and SSE wind events at CYUL. A comparison of prolonged cold-season NNE wind events with warm-season NNE wind events at CYUL would be useful to determine if pressure-driven channeling is still a dominant mechanism in the SLRV during periods of weaker stability (i.e., the warm

TABLE A1. Dates and times of the 55 synoptically independent NNE wind events at CYUL. Times are UTC.

Start date	Start time	End date	End time
11 Dec 1979	0300	11 Dec 1979	2300
5 Jan 1980	1000	6 Jan 1980	0300
15 Dec 1982	2300	19 Dec 1982	1900
23 Jan 1983	1100	24 Jan 1983	0600
7 Feb 1983	1600	8 Feb 1983	1200
11 Dec 1983	2000	12 Dec 1983	1100
30 Jan 1984	2000	31 Jan 1984	1100
11 Feb 1984	0300	11 Feb 1984	2000
17 Jan 1985	1400	18 Jan 1985	0700
25 Jan 1985	0800	26 Jan 1985	0400
31 Jan 1985	1200	1 Feb 1985	0700
3 Jan 1986	0800	4 Jan 1986	0300
4 Feb 1986	1900	5 Feb 1986	1300
3 Dec 1986	0100	3 Dec 1986	1700
16 Dec 1986	2000	17 Dec 1986	1400
9 Jan 1991	0600	9 Jan 1991	2300
16 Jan 1991	0200	16 Jan 1991	1900
18 Feb 1991	2300	19 Feb 1991	1800
7 Dec 1991	1300	8 Dec 1991	0700
29 Dec 1991	1900	30 Dec 1991	1300
31 Jan 1993	0900	1 Feb 1993	0200
5 Feb 1993	2300	6 Feb 1993	1600
12 Feb 1993	2100	13 Feb 1993	1500
8 Jan 1994	0100	8 Jan 1994	1800
9 Feb 1994	0200	9 Feb 1994	2200
23 Feb 1994	1000	24 Feb 1994	0600
2 Jan 1997	0100	2 Jan 1997	1600
9 Jan 1997	2300	10 Jan 1997	1500
24 Jan 1997	0000	24 Jan 1997	2000
11 Feb 1997	0300	11 Feb 1997	2100
14 Feb 1997	0600	14 Feb 1997	2300
10 Dec 1997	1600	11 Dec 1997	0700
15 Dec 1997	1800	16 Dec 1997	1200
29 Dec 1997	1400	30 Dec 1997	0700
4 Jan 1998	1100	5 Jan 1998	0300
7 Jan 1998	0500	7 Jan 1998	2100
23 Jan 1998	0300	23 Jan 1998	2000
27 Jan 1998	2300	28 Jan 1998	1700
20 Dec 1998	1400	21 Dec 1998	1000
3 Jan 1999	0300	3 Jan 1999	2300
15 Jan 1999	0000	15 Jan 1999	2000
11 Feb 1999	1900	12 Feb 1999	1000
24 Feb 1999	1900	25 Feb 1999	1100
6 Dec 1999	1400	7 Dec 1999	0800
2 Jan 2000	0900	3 Jan 2000	0300
23 Jan 2000	2000	24 Jan 2000	1100
31 Jan 2001	0800	1 Feb 2001	0300
9 Feb 2001	0200	9 Feb 2001	2100
23 Dec 2001	1500	24 Dec 2001	0600
15 Jan 2002	0400	16 Jan 2002	0100
29 Jan 2002	0700	30 Jan 2002	0400
17 Feb 2002	0400	17 Feb 2002	2200
25 Feb 2002	0000	25 Feb 2002	1800
16 Dec 2002	0100	16 Dec 2002	2100
25 Dec 2002	1000	26 Dec 2002	0300

TABLE A2. Dates and times of the 16 synoptically independent SSE wind events at CYUL. Times are UTC.

Start date	Start time	End date	End time
23 Feb 1979	1900	24 Feb 1979	0900
5 Dec 1979	1700	6 Dec 1979	0800
15 Dec 1979	1800	16 Dec 1979	0600
11 Jan 1980	1100	12 Jan 1980	0300
7 Jan 1981	0400	7 Jan 1981	1600
2 Feb 1981	0000	2 Feb 1981	1100
8 Feb 1981	0500	8 Feb 1981	1600
10 Feb 1981	2100	11 Feb 1981	1500
3 Dec 1982	1600	4 Dec 1982	0500
23 Dec 1985	0200	23 Dec 1985	1500
11 Jan 1986	2100	12 Jan 1986	1400
23 Jan 1991	0900	24 Jan 1991	0300
6 Jan 2000	1500	7 Jan 2000	0200
27 Feb 2000	0400	27 Feb 2000	1800
13 Dec 2001	0600	13 Dec 2001	2100
12 Feb 2002	0700	12 Feb 2002	1800

season). This would elucidate whether certain surface wind regimes are associated with preexisting low-level temperature inversions, or if the wind regimes cause the low-level temperature inversions. Mesoscale numerical modeling would potentially add useful insight to many avenues of future work. Finally, wind events and channeling at other locations within the SLRV [e.g., Quebec City (CYQB) and Massena, New York (KMSS)] should be examined as a comparison with the orographic effects observed at CYUL.

Acknowledgments. This research has been funded by grants from Mathematics of Information Technology and Complex Systems (MITACS), Ouranos, the Natural Sciences and Engineering Research Council of Canada (NSERC), and the Canadian Foundation for Climate and Atmospheric Sciences (CFCAS). Thanks are given to the National Climatic Data Center (NCDC) for providing access to the NARR and to Iowa State University and Environment Canada for their hourly surface observation datasets. Finally, many thanks are given to the three anonymous reviewers, who helped to improve the quality of this manuscript.

APPENDIX

List of Wind Events

Tables A1 and A2 give the dates and times of all NNE and SSE events, respectively, that were used in this study.

REFERENCES

Alpert, P., I. Osetinsky, B. Ziv, and H. Shafir, 2004: Semi-objective classification for daily synoptic systems: Application to the

eastern Mediterranean climate change. *Int. J. Climatol.,* **24,** 1001–1011.

Amante, C., and B. W. Eakins, 2009: ETOPO1 1 Arc-Minute Global Relief Model: Procedures, data sources and analysis. NOAA Tech. Memo. NESDIS NGDC-24, 9 pp.

Bergstrom, H., and N. Juuso, 2006: A study of valley winds using the MIUU mesoscale model. *Wind Energy,* **9,** 109–129.

Bluestein, H. B., 1992: *Synoptic-Dynamic Meteorology in Midlatitudes*. Vol. I. Oxford University Press, 431 pp.

Carrera, M. L., J. R. Gyakum, and C. A. Lin, 2009: Observational study of wind channeling within the St. Lawrence River valley. *J. Appl. Meteor. Climatol.,* **48,** 2341–2361.

Cohn, S. A., J. R. Gyakum, R. R. Rogers, W. L. Ecklund, D. A. Carter, and J. S. Wilson, 1996: Wind profiler/RASS observations of two complex synoptic events. *Beitr. Phys. Atmos.,* **69,** 37–47.

Doyle, J. D., and N. A. Bond, 2001: Research aircraft observations and numerical simulations of a warm front approaching Vancouver Island. *Mon. Wea. Rev.,* **129,** 978–998.

Fitzjarrald, D. R., and G. G. Lala, 1989: Hudson valley fog environments. *J. Appl. Meteor.,* **28,** 1303–1328.

Gabersek, S., and D. R. Durran, 2006: Gap flows through idealized topography. Part II: Effects of rotation and surface friction. *J. Atmos. Sci.,* **63,** 2720–2739.

Gross, G., and F. Wippermann, 1987: Channeling and countercurrent in the upper Rhine Valley: Numerical simulations. *J. Climate Appl. Meteor.,* **26,** 1293–1304.

Gyakum, J. R., and P. J. Roebber, 2001: The 1998 ice storm—Analysis of a planetary-scale event. *Mon. Wea. Rev.,* **129,** 2983–2997.

Jeffreys, H., 1922: On the dynamics of wind. *Quart. J. Roy. Meteor. Soc.,* **48,** 29–48.

Koch, S., M. DesJardins, and P. Kocin, 1983: An interactive Barnes objective map analysis scheme for use with satellite and conventional data. *J. Climate Appl. Meteor.,* **22,** 1487–1503.

Kossmann, M., and A. P. Sturman, 2003: Pressure-driven channeling effects in bent valleys. *J. Appl. Meteor.,* **42,** 151–158.

Ladd, J. W., and D. M. Driscoll, 1980: A comparison of objective and subjective means of weather typing: An example from west Texas. *J. Appl. Meteor.,* **19,** 691–704.

MathWorks, cited 2010: MATLAB: Introduction and key features. [Available online at http://www.mathworks.com/products/matlab/description1.html.]

McNider, R. T., and R. A. Pielke, 1984: Numerical simulation of slope and mountain flows. *J. Climate Appl. Meteor.,* **23,** 1441–1453.

Mesinger, F., and Coauthors, 2006: North American Regional Reanalysis. *Bull. Amer. Meteor. Soc.,* **87,** 343–360.

Milrad, S. M., E. H. Atallah, and J. R. Gyakum, 2009a: Dynamical and precipitation structures of poleward-moving tropical cyclones in eastern Canada, 1979–2005. *Mon. Wea. Rev.,* **137,** 836–851.

——, ——, and ——, 2009b: Synoptic-scale characteristics and precursors of cool-season precipitation events at St. John's, Newfoundland, 1979–2005. *Wea. Forecasting,* **24,** 667–689.

——, ——, and ——, 2010: Synoptic typing of extreme cool-season precipitation events at St. John's, Newfoundland, 1979–2005. *Wea. Forecasting,* **25,** 562–586.

——, J. R. Gyakum, E. H. Atallah, and J. F. Smith, 2011: A diagnostic examination of the eastern Ontario and western Quebec wintertime convection of 28 January 2010. *Wea. Forecasting,* **26,** 301–318.

Muller, R. A., 1977: A synoptic climatology for environmental baseline analysis: New Orleans. *J. Appl. Meteor.,* **16,** 20–33.

——, and A. L. Jackson, 1985: Estimates of climatic air quality potential at Shreveport, Louisiana. *J. Climate Appl. Meteor.,* **24,** 293–301.

National Climatic Data Center, cited 2008: Eastern U.S. flooding and ice storm. [Available online at http://www.ncdc.noaa.gov/oa/reports/janstorm/janstorm.html.]

Nawri, N., and R. E. Stewart, 2006: Climatological features of orographic low-level jets over Frobisher Bay. *Atmos.–Ocean,* **44,** 397–413.

Overland, J. E., and T. R. Hiester, 1980: Development of a synoptic climatology for the northeast Gulf of Alaska. *J. Appl. Meteor.,* **19,** 1–14.

Powe, N. N., 1969: The climate of Montreal. Canadian Department of Transport, Meteorology Bureau, Climatological Study 15, 51 pp. [Available from the Canadian Government Publishing Centre, Supply and Services Canada; Ottawa, ON, Canada K1A 0S9.]

Razy, A., 2010: Synoptic analysis of cold-season surface wind regimes in Montreal. M.S. thesis, Dept. of Atmospheric and Oceanic Sciences, McGill University, 102 pp.

Ressler, G. M., S. M. Milrad, E. H. Atallah, and J. R. Gyakum, 2012: Synoptic-scale analysis of freezing rain events in Montreal, Quebec. *Wea. Forecasting,* in press.

Roebber, P. J., and J. R. Gyakum, 2003: Orographic influences on the mesoscale structure of the 1998 ice storm. *Mon. Wea. Rev.,* **131,** 27–50.

Schmidli, J., G. S. Poulos, M. H. Daniels, and F. K. Chow, 2009: External influences on nocturnal thermally driven flows in a deep valley. *J. Appl. Meteor. Climatol.,* **48,** 3–23.

Sharp, J., and C. Mass, 2002: Columbia Gorge gap flow. *Bull. Amer. Meteor. Soc.,* **83,** 1757–1762.

Sharples, J., R. McRae, and R. Weber, 2009: An empirical probabilistic study of wind direction over complex terrain. *Proc. 18th World IMACS Congress and MODSIM09 Int. Congress on Modeling and Simulation,* Cairns, Australia, Modeling and Simulation Society of Australia and New Zealand and International Association for Mathematics and Computers in Simulation, 4446–4452.

Sisson, P. A., and J. R. Gyakum, 2004: Synoptic-scale precursors to significant cold-season precipitation events in Burlington, Vermont. *Wea. Forecasting,* **19,** 841–854.

Slonosky, V. C., 2003: The meteorological observations of Jean-François Gaultier, Quebec, Canada: 1742–56. *J. Climate,* **16,** 2232–2247.

Steenburgh, W. J., C. F. Mass, and S. A. Ferguson, 1997: The influence of terrain-induced circulations on wintertime temperature and snow level in the Washington Cascades. *Wea. Forecasting,* **12,** 208–227.

Sturman, A. P., 1987: Thermal influences on airflow in mountainous terrain. *Prog. Phys. Geogr.,* **11,** 183–206.

Weber, R. O., and P. Kaufmann, 1998: Relationship of synoptic winds and complex terrain flows during the MISTRAL field experiment. *J. Appl. Meteor.,* **37,** 1486–1496.

Whiteman, C. D., and J. C. Doran, 1993: The relationship between overlying synoptic-scale flows and winds within a valley. *J. Appl. Meteor.,* **32,** 1669–1682.

Wippermann, F., and G. Gross, 1981: On the construction of orographically influenced wind roses for given distributions of the large-scale wind. *Beitr. Phys. Atmos.,* **54,** 492–501.

Zhong, S., J. Li, C. D. Whiteman, X. Bian, and W. Yao, 2008: Climatology of high wind events in the Owens Valley, California. *Mon. Wea. Rev.,* **136,** 3536–3552.